

Orientation Changes in Myosin Regulatory Light Chains Following Photorelease of ATP in Skinned Muscle Fibers

Taylor St. Claire Allen,* Nicholas Ling,† Malcolm Irving,§ and Yale E. Goldman||

*Pennsylvania Muscle Institute, University of Pennsylvania, Philadelphia, Pennsylvania 19104-6083 USA, and †Randall Institute, King's College London, London WC2B 5RL, England

ABSTRACT The orientation of the light-chain region of myosin heads in muscle fibers was followed by polarized fluorescence from an extrinsic probe during tension transients elicited by photolysis of caged ATP. Regulatory light chain from chicken gizzard myosin was covalently modified with iodoacetamidotetramethylrhodamine and exchanged into skinned fibers from rabbit psoas muscle without significant effect on the tension transients. Fluorescence polarization ratios $Q_{\parallel} = (I_{\parallel} - I_{\perp}) / (I_{\parallel} + I_{\perp})$ and $Q_{\perp} = (I_{\perp} - I_{\parallel}) / (I_{\perp} + I_{\parallel})$, where $I_{m,n}$ denote fluorescence intensities for excitation (pre-subscript) and emission (post-subscript) parallel or perpendicular to the fiber axis, were simultaneously measured at 0.5 ms time resolution. Q_{\perp} decreased and Q_{\parallel} increased promptly after ATP release in the presence or absence of Ca^{2+} , indicating changes in orientation of the light-chain region associated with ATP binding or cross-bridge detachment. Little further change in the Q signals accompanied either active tension development (+ Ca^{2+}) or the final relaxation (- Ca^{2+}). The Q and tension transients slowed when liberated ATP concentration was reduced. Assuming that ATP is released at 118 s^{-1} (20°C), the apparent second-order rate constants were $3-10 \times 10^5 \text{ M}^{-1} \text{ s}^{-1}$ for Q_{\parallel} , $1-5 \times 10^5 \text{ M}^{-1} \text{ s}^{-1}$ for Q_{\perp} , and $0.5-2 \times 10^5 \text{ M}^{-1} \text{ s}^{-1}$ for the convergence of tension traces starting from different rigor values. Fitting of model orientation distributions to the Q signals indicated that the angular disorder increases after ATP binding. This orientation change is specific to ATP because photorelease of ADP caused much smaller changes in the Q signals.

INTRODUCTION

In an accompanying paper (Ling et al., 1996) we measured the polarized fluorescence of acetamidotetramethylrhodamine (ATR) probe molecules covalently bound to the regulatory light chains of myosin in rabbit psoas muscle fibers. Fluorescence polarization was determined in relaxed, rigor, and actively contracting fibers, and interpreted in terms of changes of the orientation distribution of the probes and of the underlying myosin light-chain region. According to the classic tilting-head model of force generation in muscle (Reedy et al., 1965; H. E. Huxley, 1969; Lyman and Taylor, 1971; A. F. Huxley and Simmons, 1971), such changes in angular distribution are expected when the actomyosin cross-bridges in the fiber generate force. In the steady state of contraction, the actomyosin ATPase activity generates a mixture of all of the biochemical states on the pathway of the enzymatic reaction. The orientation distribution of myosin molecules is then expected to reflect the population of several biochemical states, and the relationship between components of the orientation distribution and the individual biochemical and mechanical states is not clear.

Possible routes to isolating biochemical and mechanical intermediates of the cross-bridge cycle are the use of nucleotide analogs that mimic individual states (Yount, 1975; Reedy et al., 1983; Cooke, 1986; Thomas, 1987; Chase et al., 1993; Fisher et al., 1995; Ostap et al., 1995) and kinetic perturbations that transiently alter the population of cross-bridge states and thereby partially synchronize the cycle (Gutfreund, 1972; Huxley and Simmons, 1971; Goldman et al., 1982). Many studies have used photolysis of caged ATP in rigor muscle fibers to abruptly initiate the cross-bridge cycle (Goldman et al., 1982, 1984b; Homsher and Millar, 1990). This method has the advantages that the initial condition is biochemically homogeneous and structurally well characterized and that the mechanical and biochemical events after release of ATP have been described. Tension decreases from the rigor value for ~ 20 ms at 20°C , suggesting detachment of the cross-bridges, and then increases over the next 100–200 ms as the cross-bridges reattach and generate force (Goldman et al., 1982, 1984b). Biochemically, there is a burst of ATP hydrolysis and then slower product release and continued cycling of the ATPase reaction (Ferenczi et al., 1984; Ferenczi, 1986).

The equatorial reflections of the x-ray diffraction pattern show large changes in the intensity within 10 ms of photolysis of caged ATP, but no clear component accompanying development of active force (Poole et al., 1991; Brown et al., 1995). Electron micrographs of fibers rapidly frozen after photolysis of caged ATP show disordering of the cross-bridge shapes and angles within 12 ms of ATP release, and then much more subtle structural changes during the subsequent development of active force (Hirose et al., 1993, 1994). A large orientation change of ATR probes

Received for publication 12 September 1995 and in final form 10 January 1996.

Address reprint requests to Dr. Yale E. Goldman, Pennsylvania Muscle Institute, University of Pennsylvania, Philadelphia, PA 19104-6083. Tel.: 215-898-4017; Fax: 215-898-2653; E-mail: goldmany@mail.med.upenn.edu.

Dr. Allen's present address is Department of Cell and Developmental Biology, University of Pennsylvania, Philadelphia, PA 19104-6058.

Dr. Ling's present address is Department of Biological Sciences, University of Waikato, Private Bag 3105, Hamilton, New Zealand.

© 1996 by the Biophysical Society

0006-3495/96/04/1847/16 \$2.00

bound to Cys 707 of the myosin heavy chain occurs during the nucleotide binding and cross-bridge dissociation phases after ATP liberation, but there is little further change during active force development (Tanner et al., 1992; Berger et al., 1995). As expected from earlier static fluorescence polarization studies (Burghardt et al., 1983), ATP and ADP change the orientation of the Cys-707-ATR probes to a similar extent. The large change in ATR orientation observed with ATP or ADP is probably a local structural change near the nucleotide binding site and is not directly responsible for the force-generating transition in skeletal muscle (Tanner et al., 1992; Berger et al., 1995).

It is possible that only the light-chain region of the head undergoes large orientation changes during force development (Cooke, 1986; Thomas, 1987; Vibert and Cohen, 1988; Rayment et al., 1993) and that some of the techniques used previously to detect cross-bridge motions after photorelease of ATP are not sensitive to tilting of this limited portion of the cross-bridge. We therefore combined the technique for studying orientation and mobility of ATR probes attached to Cys 108 of regulatory light chains (Ling et al., 1996) with perturbation of the system by photolysis of caged nucleotides, and we investigated changes in the orientation of the light-chain region of the myosin heads after photolysis of caged ATP and caged ADP. We analyzed the changes in fluorescence polarization according to specific models of the orientation distribution and compared the time course of the orientation changes with that of cross-bridge detachment as signaled by tension differences between trials starting at different rigor tensions. The results have been briefly presented in abstract form (Allen et al., 1992, 1993).

MATERIALS AND METHODS

General experimental procedures

The orientation of acetamidotetramethylrhodamine (ATR) bound to myosin regulatory light chains (RLCs) in rabbit psoas muscle fibers was measured in relaxed and rigor conditions and with high time resolution after photolysis of caged ATP and caged ADP. The methods of fiber

preparation and labeling were as described in an accompanying paper (Ling et al., 1996), and the experimental setup was a modification of that described by Tanner et al. (1992). Briefly, small bundles of psoas fibers were teased from the muscle, tied to wooden sticks, and permeabilized in glycerol/ATP solution (Goldman et al., 1984a). Chicken gizzard regulatory light chains (cgRLCs), either purified from the tissue or expressed in *Escherichia coli*, were kindly provided by Dr. J. Kendrick-Jones (Cambridge, England) and were labeled in vitro using iodo-ATR purchased from Molecular Probes (Eugene, OR), lots 9B and 10A, which are probably mixtures of the 5 and 6 isomers (predominantly the 6 isomer) (Sabido-David et al., 1994). Similar results were obtained with the two probe samples. In the four protein batches used here, $38 \pm 6\%$ (mean \pm SEM) of the single cysteine (Cys 108) in the cgRLC was labeled with iodo-ATR. Single muscle fibers were mounted in the experimental apparatus and subjected to a procedure involving exchange with the exogenous cgRLC at 30°C for 30 min in a solution with low divalent cation concentrations, addition of whole troponin and then troponin-C at 10°C, and finally returning the fiber to the experimental temperature of 20°C (Moss et al., 1982). For more details on the labeling and RLC exchange procedures, including extent of labeling, extent and specificity of RLC exchange, sarcomere location of the exogenous RLC, and x-ray diffraction studies on effects of RLC exchange, see Ling et al. (1996).

Caged nucleotides were synthesized as described by Walker et al. (1988). Residual contaminants in the caged nucleotides were kept below 0.2% as detected by reverse-phase high-performance liquid chromatography. ADP (Sigma Chemical Company or Boehringer-Mannheim Biochemicals) was purified as described by Dantzig et al. (1991). Solution compositions are shown in Table 1.

Experiments were performed at room temperature (20–22°C). The solution exchanger and the experimental protocol for laser pulse photolysis of caged ATP and caged ADP are described by Tanner et al. (1992) and Goldman et al. (1984a). Briefly, single fibers were dissected and mounted with T-shaped aluminum foil clips onto hooks on a force transducer (natural frequency ~ 5 kHz) and a moving coil driver for programmed length changes. Fiber stiffness was measured using imposed 2 kHz sinusoidal length changes and software, described below, to emulate a lock-in amplifier to detect the in-phase (elastic modulus) and out-of-phase (viscous modulus, or quadrature) components of the complex 2 kHz stiffness. Sarcomere lengths and fiber dimensions were determined as described by Goldman and Simmons (1984). A typical photolysis trial beginning in 5 mM MgATP relaxing solution consisted of a 2-min incubation in 0.1 mM ATP relaxing solution, 6 min in rigor, including a second rigor wash, 5 min in rigor + Ca^{2+} , including a second rigor + Ca^{2+} wash and, finally, Ca^{2+} rigor plus 10 mM caged ATP. In some experiments (Figs. 1, 5, 7, 9, and 10) a $\sim 0.5\%$ stretch was applied 1 s before the laser pulse to increase rigor tension. For experiments with caged ADP, the fiber was put into rigor, washed again with the rigor solution, and then put into rigor plus 10 mM

TABLE 1 Solutions used during caged ATP photolysis trials (concentrations in mM)

Solution	TES	EGTA	CaEGTA	HDTA	Na_2ATP	Na_2CP	MgCl_2	Caged ATP	Caged ADP
Relax, 5 mM MgATP	100	25			5.4	19.1	7.7		
Relax, 0.1 mM MgATP	100	30			0.12	21.5	2.7		
Relax, 0.75 mM MgATP	100	20		17.58	0.86	15	3.22		
Relax, 0.75 mM + caged ATP	97.2	20			0.86	15	5.29	10	
Rigor	100	52.7					3.2		
Rigor + caged ATP	100	20		16.17			4.08	10	
Rigor + caged ADP	100	20		16.17			4.08		10
Ca^{2+} Rigor	100		20	32.6			1.3		
Ca^{2+} Rigor + caged ATP	100		20	16.63			3.3	10	

All solutions contained 10 mM reduced glutathione, 1 mM calculated free Mg^{2+} , 200 mM ionic strength at pH 7.1 and 20°C. EGTA, ethyleneglycol-bis-(β -aminoethylether)*N,N,N',N'*-tetraacetic acid; Ca-EGTA, contains the same concentrations of total Ca and EGTA; TES, *N*-tris(hydroxymethyl)methyl-2-aminoethanesulfonic acid; GSH, reduced glutathione; caged ATP, P^3 -1-(2-nitro)phenylethyladenosine 5'-triphosphate; HDTA, 1,6-diaminohexane-*N,N,N',N'*-tetracetic acid.

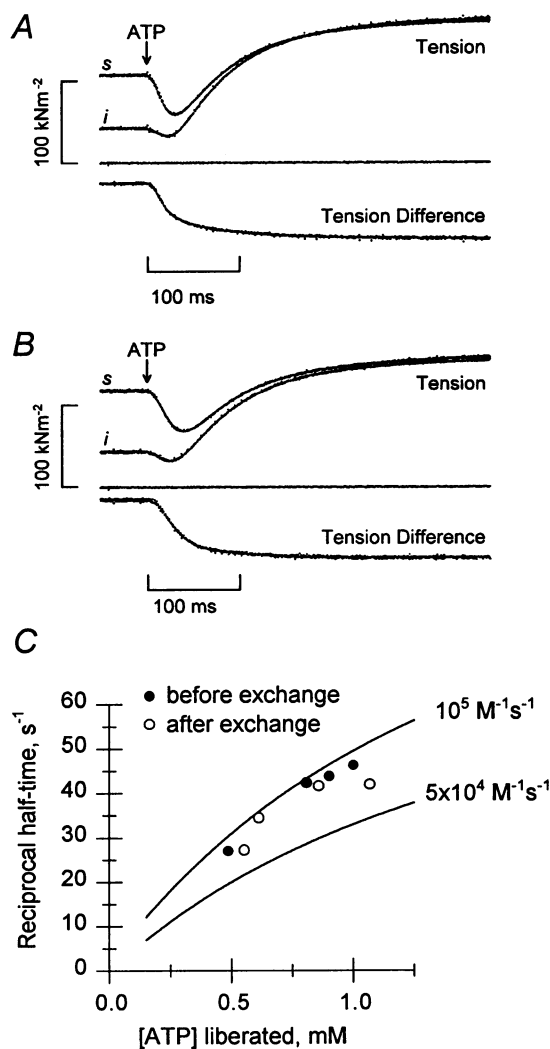
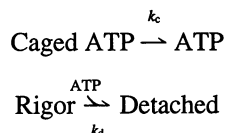


FIGURE 1 Effect of exchanging ATR-labeled chicken gizzard regulatory light chains into single rabbit psoas muscle fibers on tension transients initiated by photolysis of caged ATP. (A) Before exchange; (B) after exchange. At the arrows, 0.80 mM ATP was photoliberated in rigor solution containing 30 μM free Ca^{2+} . Each panel shows one trial in which the fiber was held isometric (*i*) and one in which the fiber was stretched (*s*) by 0.5% 1 s before the laser pulse to increase the initial rigor tension. The flat trace in each panel is the tension baseline recorded with the fiber in relaxing solution. The bottom traces (Tension Difference) are the algebraic differences between pre-stretch and isometric trials, and show the time course of convergence of the *i* and *s* traces. Half-times for tension convergence were 23.6 ms and 29.0 ms before and after RLC exchange. Sarcomere length, 2.58 μm ; fiber length, 2.18 mm; cross-sectional area, 5780 μm^2 ; $T = 10^\circ\text{C}$. (C) Reciprocal half-times for tension convergence before (●) or after (○) exchange plotted against liberated [ATP]. [MgATP] would be about 15% lower than [ATP]. The curves show the reciprocal half-times predicted from the kinetic model shown below, with the first-order rate of ATP release after the laser pulse (k_e) set to 50 s^{-1} at 10°C (Barabas and Keszthelyi, 1984), and the apparent second-order rate of cross-bridge detachment by ATP (k_d) set to either $5 \times 10^4 \text{ M}^{-1} \text{ s}^{-1}$ or $10^5 \text{ M}^{-1} \text{ s}^{-1}$, as shown to the right of the curves.



caged ADP. Photoliberation of ATP or ADP was determined by high-performance liquid chromatography of the photolyzed samples as described by Goldman et al. (1984a).

Dynamic measurement of fluorescence polarization

The setup was similar to that used by Tanner et al. (1992) to measure linear dichroism by collecting modulated total fiber fluorescence when the polarization of the fluorescence excitation was modulated at 84.2 kHz with a photoelastic modulator (PEM). The PEM acts as a variable wave plate with oscillating phase retardation. The major changes for the present fluorescence polarization experiments were the addition of a Wollaston prism to separate fluorescence emission parallel and perpendicular to the fiber axis and use of two photomultiplier tubes and two 84.2 kHz lock-in amplifiers to simultaneously detect the modulation of the parallel and perpendicular fluorescence emission.

The major components for fluorescence excitation that were kept from the previous setup (Tanner et al., 1992) are the following. A continuous, 100 mW, 514.5 nm argon ion laser (ILT, Salt Lake City, UT) had an initial polarization perpendicular to the fiber axis. Light passed through an attenuator, a photoelastic polarization modulator (Hinds International, Portland, OR), oriented with principal axis 45° from the fiber axis, a negative meniscus lens, a converging cylindrical lens, and mirrors to project the beam onto the horizontal fiber from below. The 1/e² full width of the beam was approximately 3 mm along the fiber axis and 0.5 mm across the fiber.

Changes to this system from the earlier setup were as follows. A 500 nm, 40 nm full-width half-maximum bandpass interference filter reduced orange light scattered from the arc lamp that optically pumped the argon laser cavity, allowing removal of an opaque stop at the center of the fluorescence collecting lens that had been necessary to reduce the detector background level. The peak retardation of the photoelastic modulator at $\lambda = 514.5 \text{ nm}$ was reduced from the earlier value of 0.5λ to 0.383λ as described later. The fluorescent emission was collected by a spherical achromatic lens 2.5 cm in diameter, placed 5 cm above the fiber (in line with the excitation beam), after spectral filtering by a 1-cm path of 0.1 M KCr_2O_7 , a 590-nm long-pass cut-off filter, and a 600-nm, 40-nm full-width half-maximum bandpass interference filter. The numerical collection aperture was about 0.18. The small effect of this finite aperture (<0.002 change of polarization ratio) was ignored. Parallel and perpendicular fluorescence emissions were separated by a Wollaston prism and detected with two photomultiplier tubes (model R928; Hamamatsu, Bridgewater, NJ). Phosphorescence of trough components (all metal, teflon, or fused silica) and of the optical filters was low enough to allow removal of a gating circuit previously used (Tanner et al., 1992) that had introduced a 1–2-ms detector dead time after the laser photolysis pulse. This change eliminated the dead time in the present experiments, but transient deflections of the optical signals lasting ~ 1 ms after the photolysis pulse, due to scattering of the photolysis pulse into the detectors, are present on some of the recordings (Figs. 3 B, 5 B, and 7). The waveforms of the fluorescence signals from the two photomultiplier tubes are modulated at 84.2 kHz and match the expected form $\cos(p \cdot \sin(2\pi f_p t))$, where f_p is the resonant frequency (42.1 kHz) and p is the peak optical retardation of the photoelastic modulator. The wave shape is similar to that shown in Fig. 2 of Tanner et al. (1992), except that the reduced retardation in the present case reduced the asymmetry.

Two lock-in amplifiers (Ithaco model 3961B, Ithaca, NY) were used to extract the amplitudes (D_{\parallel} and D_{\perp}) of the 84.2-kHz fluorescence modulation. The final 1-kHz output filter of the lock-in amplifiers was bypassed by picking off the signals within the instruments immediately after the synchronous detectors, giving an effective 10–90% rise time for D_{\parallel} and D_{\perp} of 500 μs . The running averages (L_{\parallel} and L_{\perp}) of the modulated fluorescence signals were extracted from the photomultiplier outputs by using 1-kHz low pass filters (model 3100F; Pacific Instruments).

Processing of the optical signals

The apparatus provides fluorescence polarization ratio signals defined as

$$Q_{\parallel} = (I_{\parallel} - I_{\perp}) / (I_{\parallel} + I_{\perp}), \quad Q_{\perp} = (I_{\perp} - I_{\parallel}) / (I_{\perp} + I_{\parallel})$$

$$P_{\parallel} = (I_{\parallel} - I_{\perp}) / (I_{\parallel} + I_{\perp}), \quad P_{\perp} = (I_{\perp} - I_{\parallel}) / (I_{\perp} + I_{\parallel}),$$

where I_n are fluorescence intensities with excitation and emission parallel and/or perpendicular to the fiber axis. The pre-subscript refers to the polarization of the excitation and the post-subscript refers to the polarization of the analyzer relative to the fiber axis. The polarization ratios provide information on the orientation distributions of the rhodamine absorption and emission dipole moments and can be rigorously interpreted by using a model of those distributions. Qualitatively, however, they relate to the tendency of absorption dipoles to be aligned parallel or perpendicular to the muscle fiber axis. A more detailed interpretation is given in the Results and Discussion.

The principle of the method used to measure the polarization ratios with high time resolution is to rapidly modulate the polarization of the exciting light with a photoelastic modulator (PEM) and to simultaneously collect emitted light polarized parallel and perpendicular to the fiber axis. The photoelastic modulator acts as a variable retardation plate with the principal axis oriented at 45° to the polarization direction of the incident beam. As shown in appendix 2 of Tanner et al. (1992), when the phase difference introduced by the photoelastic modulator between the 45° and -45° components of the beam is ϕ , the intensity of total fluorescence is $\frac{1}{2}(I_{\parallel} + I_{\perp}) + \frac{1}{2}(I_{\parallel} - I_{\perp}) \cos(\phi)$, where I_{\perp} and I_{\parallel} are the total fluorescence intensities for exciting light polarized perpendicular and parallel to the fiber axis, respectively. During operation of the photoelastic modulator, $\phi = p \cdot \sin(2\pi f_p t)$, where t is time in seconds and f_p is the excitation frequency of the modulator, 42.1 kHz, and p is the peak optical phase retardation of the PEM in radians. Noting the expansion

$$\cos(z \cdot \sin(\Omega t)) = J_0(z) + 2J_2(z) \cdot \cos(2\Omega t) + 2J_4(z) \cdot \cos(4\Omega t) + \dots,$$

where J_n is the n th order Bessel function, it follows that the observed fluorescence waveforms are composed of a time-averaged value plus modulation at even harmonics of 42.1 kHz. The time-averaged value is given by $L_{\parallel} = \frac{1}{2}(I_{\parallel} + I_{\perp}) + \frac{1}{2}J_0(p)(I_{\parallel} - I_{\perp})$ for the parallel emission channel and $L_{\perp} = \frac{1}{2}(I_{\perp} + I_{\parallel}) + \frac{1}{2}J_0(p)(I_{\perp} - I_{\parallel})$ for the perpendicular emission channel. The amplitude of the second harmonic components, at 84.2 kHz, are $D_{\parallel}' = J_2(p)(I_{\parallel} - I_{\perp})$ and $D_{\perp}' = J_2(p)(I_{\perp} - I_{\parallel})$. For convenience, we define $D_{\parallel} = -D_{\parallel}' = J_2(p)(I_{\parallel} - I_{\perp})$; the negative sign is introduced by reversing the phase reference angle of the parallel lock-in amplifier. The Q polarization ratios are related to the measured L and D quantities by

$$Q_{\perp} = D_{\perp}' / (2J_2(p)L_{\perp} - J_0(p)D_{\perp}') \quad (1)$$

and

$$Q_{\parallel} = D_{\parallel}' / (2J_2(p)L_{\parallel} + J_0(p)D_{\parallel}')$$

$J_0(p) = 0$ at $p = 2.405$, so if the peak retardation of the PEM(p) is set to 2.405 radians, the expressions for the polarization ratios simplify to

$$Q_{\perp} = \frac{1}{2}D_{\perp}' / J_2(p)L_{\perp} = a_{\perp}' D_{\perp}' / L_{\perp}$$

and

$$Q_{\parallel} = \frac{1}{2}D_{\parallel}' / J_2(p)L_{\parallel} = a_{\parallel}' D_{\parallel}' / L_{\parallel}$$

In our earlier study, we set $p = \pi$, corresponding to $\frac{1}{2}\lambda$ peak optical retardation, which caused the laser beam to be linearly polarized at 90° to the incident polarization at the peaks of the PEM oscillation cycle. With the lower setting of $p = 2.405$, corresponding to 0.383λ peak optical retardation, the laser beam is elliptically polarized at the peaks of the oscillation cycle, but the numerical processing of the waveforms is greatly simplified

by elimination of the $J_0(p)D$ terms in the denominator of the equations for Q ratios. p is set on the PEM driver electronics by a potentiometer indicating the wavelength for half-wave retardation. Thus, that dial was set to 514 nm previously and 394 nm ($= 514.5 \text{ nm} \times 2.405/\pi$) here. We checked that this setting gives the correct peak retardation by a procedure given later in this section.

For the experiments, practical scaling coefficients a_{\perp} and a_{\parallel} , corresponding to the theoretical values a_{\perp}' and a_{\parallel}' , but also including the optical collection efficiencies, the sensitivity of the photomultiplier tubes, and all instrumental gains, were determined as follows on each experimental day using an object with known fluorescence polarization. A sample of randomly oriented, immobilized rhodamine was prepared by embedding iodo-ATR in epoxy resin placed between a microscope slide and a coverslip. The polarization ratios for this sample are theoretically equal to 0.5 if probe motions are negligible in the polymer and the absorption and emission dipole moments are collinear (Weber, 1952; Chen and Bowman, 1965). In an independent fluorescence polarization microscope using static polarizers, similar to that of Ling et al. (1996), the polarization ratios for the random sample ($Q_r = Q_{\parallel} = Q_{\perp} = P_{\parallel} = P_{\perp}$) were 0.476, corresponding to an approximately 11° average angle between the absorption and emission dipoles, in agreement with Ling et al. (1996). The random orientation of the sample was verified by rotating it on the stage of this microscope. The deviation of Q_r from 0.5 is caused by degeneracy of the dipole moments, incomplete immobilization of the iodo-ATR in the epoxy, or instrumental imperfections.

We placed the random sample in the PEM setup and recorded the D and L optical signals as with a fiber. From the digitized signals the scaling coefficients were calculated as $a_{\perp} = Q_r L_{\perp} / D_{\perp}$, $a_{\parallel} = Q_r L_{\parallel} / D_{\parallel}$, and $a_{\perp\parallel} = L_{\parallel} / L_{\perp}$, the relative overall gain of the parallel and perpendicular detector channels. This procedure was performed on each experimental day to obtain values for the scaling coefficients and to check the alignment of the optics and the operation of the instrumentation. Because the sine of the $J_0(p)D$ term is different for Q_{\parallel} and Q_{\perp} (see Eq. 1), an independent estimate of $J_0(p)$ is given by $(a_{\perp} - a_{\parallel} \cdot b_{\perp}/b_{\parallel}) / [Q_r(a_{\perp} + a_{\parallel} \cdot b_{\perp}/b_{\parallel})]$, where $b_{\perp}/b_{\parallel} = D_{\perp}' / L_{\perp}$, the relative overall gain of the signals (D_{\perp}' / L_{\perp}) / ($D_{\parallel}' / L_{\parallel}$). b_{\perp}/b_{\parallel} was found to be within 5% of 1.0 by comparing a_{\perp} and a_{\parallel} values obtained as normal with those measured after switching the signal cables from the two photomultiplier tubes. $J_0(p)$ was found to be typically 0.02, verifying the correct setting of the peak PEM retardation.

Using the practical scaling coefficients obtained from the random sample, the Q polarization ratios were calculated as $Q_{\parallel} = a_{\parallel} D_{\parallel}' / L_{\parallel}$ and $Q_{\perp} = a_{\perp} D_{\perp}' / L_{\perp}$. P_{\parallel} and P_{\perp} can also be calculated from the experimental quantities, but Q_{\perp} and Q_{\parallel} are more reliable because the Q ratios are each derived from only one of the photomultiplier signals and their values do not depend on the relative detector channel gain, $a_{\perp\parallel}$. We quote results as Q ratios in this paper.

Data collection and analysis

Tension, in-phase and out-of-phase stiffness, and the four optical signals (D_{\parallel} , L_{\parallel} , D_{\perp} , and L_{\perp}) were simultaneously sampled, digitized at 12-bit resolution and 500- μ s sampling rate, and stored on disk using a 80386-based computer. For stiffness measurements, a 2 kHz 0.2% sinusoidal length change was applied continuously to the fiber. A digital oscilloscope (Nicolet 3091), interfaced to an 80286-based computer, recorded the tension signal and a 2-kHz reference sinewave at a 100- μ s sampling rate. A computer program, written in house, demodulated the stiffness signals from the sinusoidal component superimposed on tension. The software generated a fixed amplitude reference sinewave either in phase or 90° out of phase with the recorded reference trace. This fixed amplitude reference was multiplied point by point with the tension data, and the product was filtered successively by recursive (Rader and Gold, 1967) 2-kHz and 4-kHz notch filters, a 100-Hz low-pass filter, and a 151-point, second-order transversal filter (Savitzky and Golay, 1964). The effective rise time (10–90%) of the stiffness signals, set by these filters, is 7 ms. The complex modulus formed by the two demodulated signals was rotated in complex space to set quadrature stiffness to zero in rigor. For the tension traces

plotted in the figures, sinusoidal components were removed by a 2-kHz, $Q = 0.5$, recursive notch filter.

Fluorescence polarization ratios were calculated off-line from the digitized signals after subtracting small background signal levels obtained with the illumination blocked and using the scaling factors obtained with a random, immobilized sample of iodo-ATR as described above. For steady-state measurements, 1 s of data (2000 samples) was averaged before the ratios were calculated. For dynamic experiments, background was subtracted and then polarization ratios were calculated point by point with the same scaling coefficients. Half-times of the transients were measured from the calculated polarization ratio signals. Exponential fitting used the Marquardt algorithm (Press et al., 1992). To reduce noise, the Q traces plotted in the figures were filtered through an 11-point, second-order transversal smoothing filter (Savitzky and Golay, 1964), leading to a 2-ms effective rise time (10–90%).

Rhodamine orientation distributions were estimated using the gaussian model and the helix plus isotropic model described by Ling et al. (1996). Adjustable parameters in these models that describe the orientation distribution were estimated by fitting the model curves to experimental Q_{\perp} and Q_{\parallel} values using scripts written in the MathCad mathematical spreadsheet software (Mathsoft Corp., Cambridge, MA). For experiments in which the time course of model fitted parameters was estimated, Q_{\perp} and Q_{\parallel} signals were averaged from several experiments to reduce noise, and the model was fitted to the average trace point by point by using a MathCad routine.

RESULTS

Effect of regulatory light-chain exchange on tension changes after ATP release

Replacement of about half of the endogenous regulatory light chains by acetamidotetramethylrhodamine-labeled chicken gizzard regulatory light chain (ATR-cgRLC) has little effect on isometric tension (Ling et al., 1996) or the tension transients after rapid length steps (Irving et al., 1995). The tension transients elicited by photolysis of caged ATP in a rigor fiber were similarly insensitive to RLC exchange (Fig. 1). Both before and after exchange (*A* and *B*, respectively), two photolysis trials were performed, one with the fiber held at fixed length (*i*) and the other with the fiber stretched (*s*) by 0.5% of its length 1 s before the photolysis laser pulse. ATP release in the presence of Ca^{2+} caused tension to first decrease, indicating cross-bridge detachment, then to increase to the plateau of active force development (Goldman et al., 1984b). After about 50 ms following the laser pulse, the tension traces from the iso-

metric and pre-stretch trials had similar time courses. The difference between the two traces (Tension Difference) provides a convenient measure of the initial detachment of rigor cross-bridges from actin; the reciprocal half-time of this signal is plotted against the concentration of released ATP in Fig. 1 C. The solid lines show the relation predicted from a simple model in which ATP release occurs in a first-order process (50 s^{-1} at 10°C ; Barabas and Keszthelyi, 1984) after the laser pulse, and ATP binding leads to detachment of the rigor cross-bridges with the second-order rate constant shown to the right of each line (Goldman et al., 1984b). The reciprocal half-times obtained before and after RLC exchange (*filled* and *open circles*, respectively) had a similar dependence on released [ATP], consistent with a second-order rate constant of slightly less than $10^5 \text{ M}^{-1} \text{ s}^{-1}$ in this model.

The rate of tension development before and after RLC exchange was compared by measuring the half-time ($t_{1/2}$) from the minimum of the tension dip after photolysis to the plateau tension value in isometric trials. $t_{1/2}$ averaged $68 \pm 3 \text{ ms}$ (mean \pm SEM, $n = 4$ trials in two fibers) before exchange and $68 \pm 2 \text{ ms}$ after exchange, indicating no significant effect of RLC exchange. Plateau tension was slightly ($\sim 10\%$) lower after exchange in these fibers.

Steady-state polarization ratios from fibers in rigor and in relaxing conditions

Fluorescence polarization ratios measured with the photoelastic modulator (PEM) as described in Materials and Methods were similar to those determined with static polarizers and reported in a companion paper (Ling et al., 1996). In 5 mM MgATP relaxing solution, Q_{\parallel} and Q_{\perp} measured using the PEM were 0.348 ± 0.002 and 0.460 ± 0.001 , respectively (mean \pm SEM; Table 2). These values are in good agreement with the corresponding values obtained with static polarizers (Ling et al., 1996), using the same batch of labeled RLC, 0.355 ± 0.008 and 0.446 ± 0.009 , respectively ($n = 7$). In rigor the PEM method gave Q_{\parallel} and Q_{\perp} values of 0.165 ± 0.005 and 0.521 ± 0.003 , respectively (Table 2), compared with 0.212 ± 0.009 and

TABLE 2 Steady-state polarization ratios

Solution	<i>n</i>	$Q_{\parallel} \pm \text{SEM}$	$Q_{\perp} \pm \text{SEM}$	Gaussian		Helical + isotropic	
				θ_0	σ	θ	<i>f</i>
Relax, 5 mM MgATP	115	0.348 ± 0.002	0.460 ± 0.001	50.7	37.2	66.9	0.788
Relax, 0.75 mM MgATP	6	0.372 ± 0.006	0.465 ± 0.004	*46.9	*48.8	69.2	0.834
Relax, 0.75 mM + caged ATP	6	0.337 ± 0.009	0.479 ± 0.001	53.7	43.5	68.7	0.751
Relax, 0.1 mM MgATP	10	0.385 ± 0.003	0.439 ± 0.003	43.6	42.2	65.5	0.884
Rigor	24	0.165 ± 0.005	0.521 ± 0.003	62.9	23.1	67.9	0.455
Rigor + caged ATP	15	0.166 ± 0.006	0.519 ± 0.004	62.7	23.0	67.8	0.457
Ca^{2+} Rigor	52	0.162 ± 0.003	0.528 ± 0.003	63.4	23.5	68.3	0.449
Ca^{2+} Rigor + caged ATP	57	0.157 ± 0.004	0.532 ± 0.002	63.8	23.5	68.5	0.441

Polarization ratios given are means \pm standard errors of the mean. The definitions of the fitted model parameters, θ_0 , σ , θ , and *f*, are given in the Discussion. The half-width (δ) of the fast-wobble cone was set to 20° , except for the values indicated with an asterisk, which were fitted using $\delta = 19^{\circ}$ because the Q values could not be fitted with $\delta = 20^{\circ}$.

0.503 ± 0.015 from the static polarizer method. The higher value of Q_{\parallel} in rigor with the static polarizer method may reflect a small error in one of the set-ups that is more significant for small Q values, or a difference between the fiber batches used for the two sets of measurements.

In rigor, Q_{\parallel} was much lower than Q_{\perp} , indicating a strong preference of the rhodamine absorption dipoles for orientations greater than 54.7° to the fiber axis, in agreement with the results in the companion paper (Ling et al., 1996). There was no significant effect of either 10 mM caged ATP or an increase in the free Ca^{2+} concentration from $\sim 10^{-10}$ M to ~ 30 μM on the rigor polarization ratios (Table 2). The difference between Q_{\parallel} and Q_{\perp} decreased slightly as the MgATP concentration of the relaxing solution was reduced from 5 mM to 100 μM (Table 2). In the presence of 0.75 mM ATP, addition of 10 mM caged ATP caused a slight decrease in Q_{\parallel} and an increase in Q_{\perp} (Table 2). In relaxed fibers the difference between Q_{\parallel} and Q_{\perp} was small, indicating that the preference of the absorption dipoles for orientations perpendicular to the fiber axis is not as strong, or that the orientations are more disordered.

Fluorescence polarization signals after photorelease of ATP

When about 2 mM ATP was released from caged ATP, Q_{\perp} decreased and Q_{\parallel} increased (Fig. 2), both in the presence of Ca^{2+} (Fig. 2 A) and in the absence of Ca^{2+} (Fig. 2 B), as expected from the steady-state results (Table 2). Mean values of Q_{\perp} and Q_{\parallel} before and after photolysis for experiments in which an average of 0.75 mM ATP was released are shown in Table 3. In the absence of Ca^{2+} there was no significant difference between Q values measured 1 s and 2 min after photolysis, and both were similar to the values measured in relaxing solution containing 0.75 mM ATP plus 10 mM caged ATP (Table 2), suggesting that there was no effect of photolysis byproducts on the Q values.

Polarization ratios in active contraction after photolysis were very similar to those in relaxation, as reported by Ling et al. (1996), but the difference between Q_{\perp} and Q_{\parallel} was

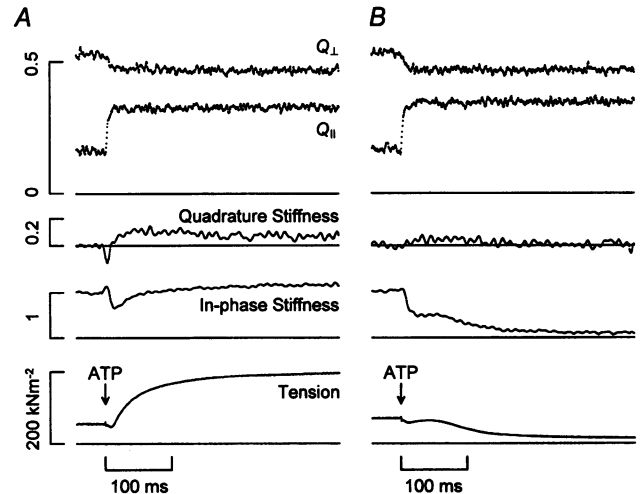


FIGURE 2 Transients of fluorescence polarization ratios, stiffness, and tension initiated by photorelease of 2.1 mM ATP from caged ATP (arrows) in the presence of ~ 30 μM free Ca^{2+} (A) and in the absence of Ca^{2+} (B). Fluorescence polarization ratios, Q_{\perp} and Q_{\parallel} , were obtained from 84.2 kHz-modulated photomultiplier signals as described in Materials and Methods. A $\leq 0.05\%$, 2 kHz sinusoidal length change was applied to the fiber for stiffness measurements, and the tension, in-phase stiffness, and quadrature (90° out-of-phase) stiffness were extracted from the force recording as described in Materials and Methods. The lowest flat line is the tension baseline recorded in relaxing solution. The other flat lines indicate zero polarization ratio, in-phase stiffness, and quadrature stiffness. The scale bar for quadrature stiffness indicates magnitude relative to in-phase stiffness just before the laser pulse. Sarcomere length, 2.48 μm ; fiber length, 2.65 mm; cross-sectional area, 5650 μm^2 ; $T = 20.4^{\circ}\text{C}$.

slightly greater in the presence of Ca^{2+} , suggesting a greater preference for probe orientations perpendicular to the fiber axis. The values of Q_{\parallel} and Q_{\perp} obtained here during contraction (bottom line of Table 3) are somewhat different numerically from those measured at the same labeling site in standard activating solution without caged ATP ($Q_{\parallel} = 0.245$, $Q_{\perp} = 0.415$, Irving et al. (1995), $T = 10^{\circ}\text{C}$; $Q_{\parallel} = 0.340$, $Q_{\perp} = 0.421$, Ling et al. (1996), $T = 10^{\circ}\text{C}$). The difference may relate to the different temperatures, batches

TABLE 3 Polarization ratios during photolysis experiments

Condition	n	$Q_{\parallel} \pm \text{SEM}$	$Q_{\perp} \pm \text{SEM}$	Gaussian		Helical + isotropic	
				θ_0	σ	θ	f
Rigor + caged ATP							
Pre-flash	9	0.175 ± 0.008	0.517 ± 0.004	62.5	23.4	67.8	0.469
Post-flash	9	0.332 ± 0.006	0.469 ± 0.004	53.1	36.1	67.5	0.749
2' post	9	0.327 ± 0.005	0.472 ± 0.005	53.7	35.8	67.6	0.737
Ca^{2+} rigor + caged ATP							
Pre-flash	14	0.171 ± 0.007	0.515 ± 0.002	62.4	23.0	67.7	0.465
Post-flash	14	0.313 ± 0.005	0.475 ± 0.003	55.0	33.4	67.4	0.708

Polarization ratios given are means \pm standard errors of the mean. Pre-flash indicates measurements in the caged ATP solution before triggering of the photolysis laser pulse. Post-flash in the absence of Ca^{2+} indicates 0.9–1 s after the laser pulse. Two minutes after the laser pulse is indicated by 2' post. Post-flash in the presence of Ca^{2+} indicates the values at peak deflection after the laser pulse. Approximately 1 mM ATP was released from caged ATP by each laser pulse. Definitions of the fitted model parameters, θ_0 , σ , θ , and f, are given in the Discussion. For fitting the models, the half-width (δ) of the fast-wobble cone was set to 20° .

of labeled RLC used, or ATP concentrations or to the presence of caged ATP in the present experiments.

When ATP was released in a rigor fiber Q_{\perp} and Q_{\parallel} changed very quickly. In the experiment of Fig. 2 ($T = 20^{\circ}\text{C}$), the half-times for the increase in Q_{\parallel} were 3.6 and 3.0 ms in the presence and absence of Ca^{2+} , respectively. The corresponding half-times for the decrease in Q_{\perp} were 7.7 and 6.4 ms. The changes in the Q signals were largely complete by the end of the initial fall of tension and in-phase stiffness seen in both the presence and absence of Ca^{2+} . Little further change in the fluorescence polarization signals accompanied either active tension development (Fig. 2 A) or relaxation (Fig. 2 B), occurring over the next 100–200 ms. In some fibers in which more than 1.7 mM ATP was released in the presence of Ca^{2+} , there were small components of the changes in Q_{\perp} and Q_{\parallel} with approximately the same time course as tension development, but their amplitude was less than 15% of the overall signal change. The increase of quadrature stiffness after photolysis from its zero value in rigor preceded active tension development (Horiuti et al., 1992) but was slower than the fluorescence polarization changes. The kinetics of the Q signals indicate that the change in orientation of the light-chain probes is associated with ATP binding to the cross-bridges or their initial detachment from actin, rather than with production of active force in the presence of Ca^{2+} , or the final relaxation in the absence of Ca^{2+} .

The fluorescence polarization ratios changed more slowly at lower concentrations of liberated ATP. When 0.28 mM ATP was released (Fig. 3), the half-time for the increase in Q_{\parallel} was 11.8 ms, and that for the decrease in Q_{\perp} was 20.7 ms, but the main deflections still clearly preceded active tension development. As described above (Fig. 2) for higher [ATP], quadrature stiffness rose more quickly than tension,

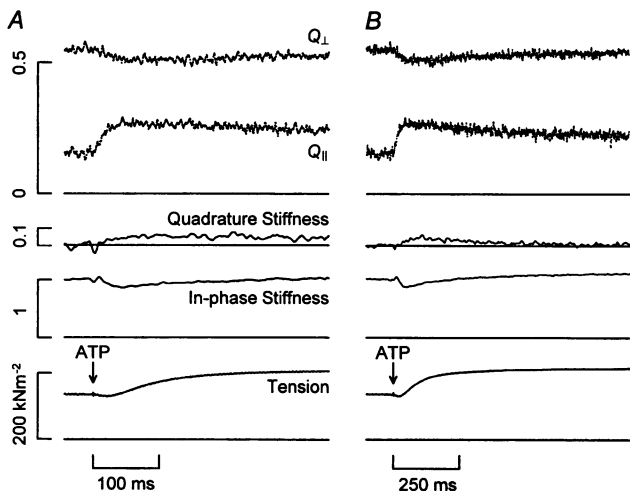


FIGURE 3 Transients of fluorescence polarization ratios, stiffness, and tension, initiated by photorelease of 0.28 mM ATP from caged ATP (arrows) in the presence of $\sim 30 \mu\text{M}$ free Ca^{2+} . The same traces are plotted at two different time bases in A and B. Sarcomere length, $2.41 \mu\text{m}$; fiber length, 3.0 mm; cross-sectional area, $5280 \mu\text{m}^2$; $T = 21.6^{\circ}\text{C}$.

but more slowly than the fluorescence polarization changes. After the initial increase of Q_{\parallel} and decrease of Q_{\perp} , both optical traces recovered slowly toward their rigor values. This recovery was observed consistently at such low concentrations of photoreleased ATP and was presumably caused by hydrolysis of the ATP by actomyosin and accumulation of ADP. When higher concentrations of ATP were released, the recovery of the polarization ratios was greatly reduced (less than 0.02 by 1 s after photorelease of $\geq 2 \text{ mM}$ ATP).

The peak amplitudes of the changes in Q_{\parallel} and Q_{\perp} were reduced at low concentrations of released ATP (compare Figs. 2 and 3). This effect is seen more clearly in Fig. 4 A, where the peak changes are plotted against liberated [ATP]. The relationship was steepest at [ATP] less than 0.4 mM, when some of the myosin heads in the fiber may not have bound ATP after photolysis and therefore would have remained in the rigor orientation. The peak change was relatively insensitive to [ATP] liberated above about 1 mM. The amplitudes of the change in Q_{\parallel} were somewhat larger for relaxation by photorelease of ATP in the absence of Ca^{2+}

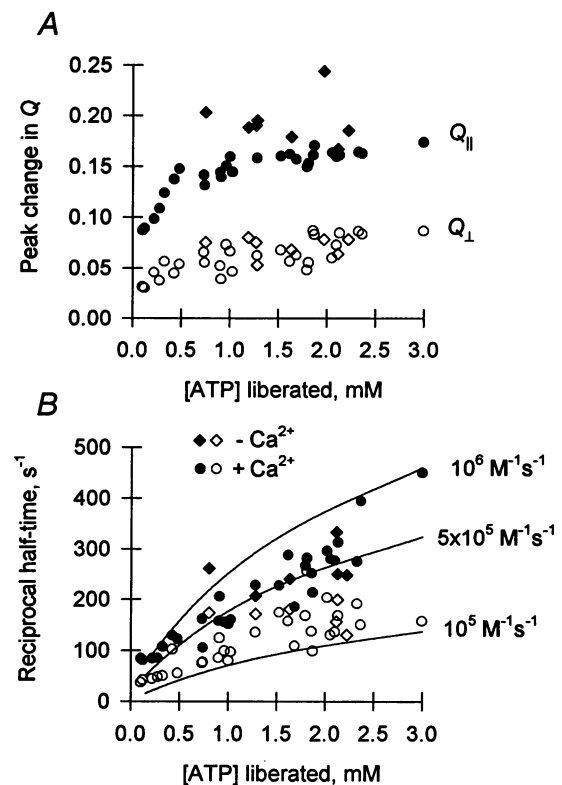


FIGURE 4 Amplitude (A) and reciprocal half-time (B) of changes in polarization ratios plotted against the concentration of liberated ATP for a series of seven fibers. \blacklozenge , Q_{\parallel} in the absence of Ca^{2+} ; \bullet , Q_{\parallel} in the presence of Ca^{2+} ; \diamond , Q_{\perp} in the absence of Ca^{2+} ; \circ , Q_{\perp} in the presence of Ca^{2+} . The curves in B show the reciprocal half-time predicted from the kinetic model in the legend to Fig. 1, with the first-order rate of ATP release after the laser pulse (k_e) set to 118 s^{-1} at 20°C (Goldman et al., 1984a,b), and the apparent second-order rate constants for cross-bridge detachment by ATP (k_d) shown to the right of each curve.

(Fig. 4 A, *filled diamonds*) than for activation by photolysis in the presence of Ca^{2+} (*filled circles*).

The fluorescence polarization signals changed more rapidly when more [ATP] was liberated throughout the range tested (100 μM to 3 mM), with no indication of saturation (Fig. 4 B). There was no clear effect of $[\text{Ca}^{2+}]$ on the measured half-times. Applying the simple kinetic model for ATP release and binding described above (Fig. 1, but ATP is released at 118 s^{-1} at 20°C), the observed reciprocal half-times were found to be consistent with apparent second-order rate constants of about $3\text{--}10 \times 10^5 \text{ M}^{-1} \text{ s}^{-1}$ for Q_{\parallel} (*filled symbols*) and about $1\text{--}5 \times 10^5 \text{ M}^{-1} \text{ s}^{-1}$ for Q_{\perp} (*open symbols*).

In some experiments the total fluorescence intensity of the probes (L), approximated by the relation $L = \parallel I_{\parallel} + 2_{\perp} I_{\perp} + 2 \parallel I_{\perp} + (8/3)_{\perp} I_{\perp}$, decreased by 5–10% promptly at the laser pulse. This decrease was not due to irreversible bleaching of the probe molecules, because when the fiber was put into rigor again for another photolysis trial, the intensity recovered to the original level. However, in other fibers L changed by less than 1% on photolysis. The intensity change observed in some fibers may be a movement artifact, or it might signal a change in the microscopic environment of the probe molecules that alters the fluorescence quantum yield. Small movements of the fiber would not affect the Q signals, because they are ratiometric.

Relative time course of the polarization signals and tension convergence

The time course of the convergence between tension traces in photolysis trials starting from different levels of rigor tension has been used as a measure of the time course of the initial detachment of rigor cross-bridges from actin (Fig. 1; see also Goldman et al., 1984a,b). We compared the time courses of tension convergence and the Q signals in paired photolysis trials, one in which the fiber was held isometric in rigor (tension traces labeled *i* in Fig. 5), and the other in which a 0.5% stretch was applied 1 s before the photolysis pulse (traces labeled *s*). The stretch had a small effect on the Q ratios in rigor; Q_{\perp} increased by 0.007 ± 0.002 and Q_{\parallel} increased by 0.012 ± 0.003 (mean \pm SEM, $n = 12$). In time-resolved measurements using purified RLC labeled with a single rhodamine isomer (Irving et al., 1995), stretches of 0.35% in rigor produced an increase in Q_{\perp} of 0.015 and, in contrast to the present results, a decrease in Q_{\parallel} of 0.006. The different effects of stretch on the polarization ratios may be related to either the rhodamine isomer or the experimental protocol.

When ATP was released the changes in both polarization ratios were faster than tension convergence (Fig. 5). When 1.85 mM ATP was released (Fig. 5 A) the tension difference decayed with a half-time of 13.1 ms, appreciably greater than those of the changes in either Q_{\perp} (3.9 ms and 5.1 ms in the isometric and pre-stretch trials, respectively) or Q_{\parallel} (3.6 ms in both trials). Similarly, when 0.41 mM ATP was

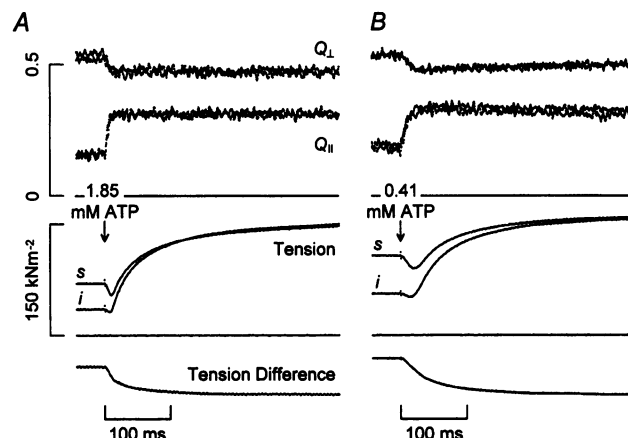


FIGURE 5 Comparison of changes in polarization ratios and tension convergence after liberation of either 1.85 mM (A) or 0.41 mM (B) ATP in the presence of 30 μM free Ca^{2+} . The middle pair of traces in each panel show tension responses in isometric (*i*) and 0.5% pre-stretch (*s*) trials, as in Fig. 1. The upper traces show Q_{\perp} and Q_{\parallel} superimposed for the *i* and *s* trials. Fiber dimensions in A: sarcomere length, 2.41 μm ; fiber length, 2.6 mm; cross-sectional area, 5900 μm^2 ; $T = 21.3^\circ\text{C}$. Fiber dimensions in B: sarcomere length, 2.38 μm ; fiber length, 2.6 mm; cross-sectional area, 3460 μm^2 ; $T = 21.1^\circ\text{C}$.

liberated (Fig. 5 B) the half-time for tension convergence was 34.5 ms, those for Q_{\perp} were 8.3 ms and 10.4 ms in the isometric and pre-stretch trials, and those for Q_{\parallel} were 7.7 ms (isometric) and 8.3 ms (pre-stretch).

Reciprocal half-times for changes in polarization ratios and for tension convergence are plotted against the concentration of liberated ATP in Fig. 6. The pre-stretch (*squares*) had little effect on the time course of the Q signals. The apparent second-order rate constants for Q_{\perp} (*open symbols*) and Q_{\parallel} (*filled symbols*) are similar to those shown previously in Fig. 4, but that for tension convergence (*triangles*)

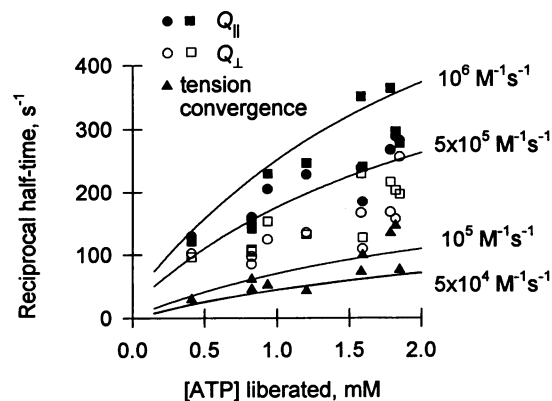


FIGURE 6 Reciprocal half-times of changes in polarization ratios and of tension convergence plotted against liberated ATP concentration. ●, Q_{\parallel} in isometric trials; ■, Q_{\parallel} in pre-stretch trials; ○, Q_{\perp} in isometric trials; □, Q_{\perp} in pre-stretch trials; ▲, convergence of tension traces from isometric and pre-stretch trials. The concentration of ATP plotted represents the average value liberated in the isometric and pre-stretch trials. The curves show predicted reciprocal half-times calculated as in Fig. 4 B for the apparent second-order rate constants shown to the right of each curve.

is clearly lower, between $5 \times 10^4 \text{ M}^{-1} \text{ s}^{-1}$ and $2 \times 10^5 \text{ M}^{-1} \text{ s}^{-1}$.

Photorelease of ATP in the presence of ADP

When MgADP is added to the rigor solution, the tension transients produced by photolysis of caged ATP are slowed, suggesting that the rate of cross-bridge detachment is reduced (Dantzig et al., 1991). Addition of MgADP also slowed the Q transients (Fig. 7). Here 1.7 mM ATP was released in the presence of 200 μM MgADP, and the half-time of the tension difference trace was increased to 24.9 ms (cf. Fig. 5). The changes in polarization ratios were slower than in the absence of MgADP but still much faster than tension convergence: in Fig. 7 Q_{\parallel} changed with a half-time of 4.4 ms in the isometric case and 6.7 ms in the pre-stretch case; Q_{\perp} changed with a half-time of 6.5 ms (isometric) and 10.5 ms (pre-stretch). When 2 mM ATP was liberated in the presence of 500 μM MgADP (not shown), the half-times were 31.7 ms for tension convergence, 7.7 ms (isometric) and 7.8 ms (pre-stretch) for Q_{\parallel} , and 12.8 ms (isometric) and 14.2 ms (pre-stretch) for Q_{\perp} . Thus the temporal dissociation between tension convergence and changes in polarization ratios is maintained when ATP binding is very slow.

Photorelease of ADP

To test whether the fluorescence polarization changes described above are specific effects of ATP, we studied the transients initiated by the photolysis of caged ADP (Fig. 8). A small fast tension decrease, by $16.0 \pm 1.2\%$ (mean \pm SEM, $n = 4$), followed the liberation of 1.5 mM ADP, as

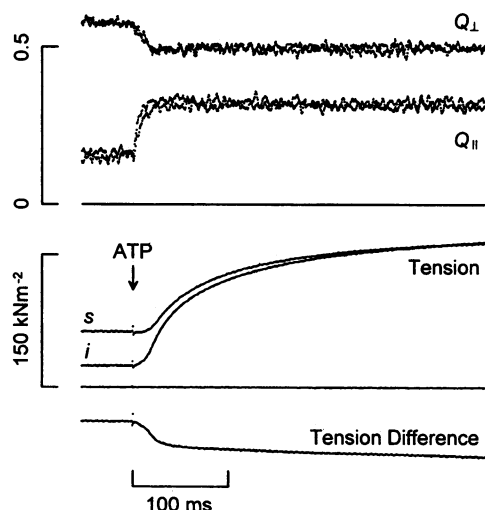


FIGURE 7 Tension convergence and changes in polarization ratios after liberation of 1.69 mM ATP in the presence of $\sim 30 \mu\text{M}$ free Ca^{2+} and 200 μM MgADP. The middle pair of traces shows tension responses in isometric (*i*) and pre-stretch (*s*) trials. The upper set of traces shows Q_{\perp} and Q_{\parallel} superimposed for the *i* and *s* trials. Sarcomere length, 2.41 μm ; fiber length, 2.6 mm; cross-sectional area, 5900 μm^2 ; $T = 21.3^{\circ}\text{C}$.

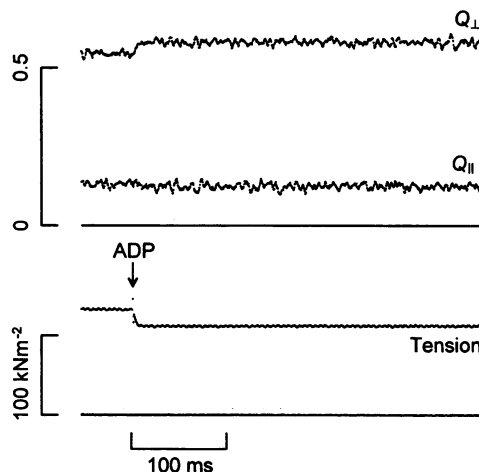


FIGURE 8 Changes in polarization ratios and tension following liberation of 1.5 mM ADP in the absence of Ca^{2+} . Sarcomere length, 2.41 μm ; fiber length, 3.0 mm; cross-sectional area, 5280 μm^2 ; $T = 21.6^{\circ}\text{C}$.

described previously (Dantzig et al., 1991). Q_{\perp} increased by 0.035 ± 0.004 from a pre-photolysis value of 0.546 ± 0.005 . There was a very small decrease in Q_{\parallel} in some fibers and no change in others; the mean decrease was 0.007 ± 0.004 from a pre-photolysis value of 0.170 ± 0.015 . These changes are much smaller and in the opposite direction of those observed after liberation of ATP, indicating that the signal changes shown in Figs. 2–7 are specific to ATP.

DISCUSSION

Fluorescence polarization from light-chain probes in muscle fibers

Rhodamine probes bound to the regulatory light chain (RLC) of myosin within muscle fibers changed their orientation promptly when ATP was released from caged ATP. The orientation change was detected using polarized fluorescence, which can be followed with submillisecond time resolution and combined with simultaneous mechanical measurements on single muscle fibers (Irving et al., 1995). The orientation distribution of the probes is not completely defined by the polarized fluorescence measurements, but the signals can be interpreted quantitatively by using specific models of the distribution. Some other limitations of the technique as used in the present work are 1) commercial samples of the rhodamine derivative used to label the RLC, iodoacetamidotetramethylrhodamine (iodo-ATR), contain a mixture of two different isomers; 2) the ATR probes undergo restricted mobility on the fluorescence time scale, probably indicating some independent mobility of the probes or small peptide segments relative to the bulk of the protein; and 3) there are alterations of the fiber structure after exchange of the labeled for the endogenous RLC (Ling et al., 1996).

The two isomers of ATR can take up different orientations in the fiber, but the polarization ratios reported above

suggest that the batches of iodo-ATR used here contained predominantly the 6-isomer (Sabido-David et al., 1994). The polarization transients after caged ATP photolysis described here are also very similar to those obtained by using cgRLC labeled with pure 6-ATR (Corrie and Craik, 1994; Hopkins et al., 1995).

In a model-dependent analysis (Irving, 1996), probe re-orientation on the nanosecond time scale of the fluorescence lifetime or faster is approximated by rapid tumbling of the fluorophore within a cone. The cone axes are considered to adopt axial and azimuthal orientation distributions that are static on the fluorescence time scale. The extent of the rapid motion can be estimated by measuring polarization ratios with different angles between the excitation and emission light beams; preliminary measurements using two excitation directions with the 6-ATR-cgRLC probe are consistent with subnanosecond motions restricted to a cone with a semi-angle of about 20° in relaxed, rigor, and actively contracting fibers (S. Hopkins, J. Shifman, M. Irving, and Y. E. Goldman, personal communication). Partitioning the probe motions into fast and slow components (Irving, 1996) allows changes in the orientation of the cone axes on the millisecond time scale after photolysis of caged ATP, to be measured in the presence of the subnanosecond probe motions, as described in detail below.

Changes in fiber structure after RLC exchange have been detected using x-ray diffraction. Ling et al. (1996) found that exchange of ATR-labeled cgRLC for the endogenous RLC leads to loss of the helical order of the myosin filaments in relaxed but not in rigor fibers. It is not known whether the x-ray pattern of actively contracting fibers is altered by RLC exchange. In the present experiments, fibers were typically activated from the rigor state by ATP release. The mechanical response to release of ATP was little altered by the RLC exchange (Fig. 1), suggesting that the functional effects of any structural changes are minor.

Quantitative interpretation of fluorescence polarization ratios

With a cylindrically symmetrical distribution of probe orientations, the fluorescence polarization signals measured with the present optical configuration are sensitive only to the angle between the muscle fiber axis and the absorption and emission dipoles of the probes (the axial angles). Azimuthal motions around the fiber axis are not detected. Because axial tilting of attached myosin heads could cause force generation or filament sliding, this specific dependence on axial angles is an advantage. The technique provides good time resolution—500 μ s in the experiments reported here and 40 μ s in other work (Irving et al., 1995).

In an earlier time-resolved study of fibers labeled with ATR on Cys 707 of the myosin heavy chain, the time course of a single observable, linear dichroism, was used to follow changes in probe orientation (Tanner et al., 1992). The two independent signals reported here, Q_{\parallel} and Q_{\perp} , provide more

information about the distribution of probe orientations, although a complete description of the distribution would require more than two parameters. A third independent signal (e.g., $P_{\parallel} = (I_{\parallel} - I_{\perp}) / (I_{\parallel} + I_{\perp})$ or $P_{\perp} = (I_{\perp} - I_{\parallel}) / (I_{\perp} + I_{\parallel})$) can be determined, but the P ratios obtained by the present method are less reliable than the Q ratios. In measurements with static polarizers, the corresponding P and Q ratios had similar values (Ling et al., 1996), as expected if the angle between the absorption and emission dipoles of ATR is small (Chen and Bowman, 1965). Therefore, P_{\parallel} and P_{\perp} do not provide substantial extra information about the ATR-RLC probe orientations.

To interpret the Q ratios in terms of probe angles, we fitted two models of the orientation distribution to the data: 1) a single population of probes with a peak angle (θ_0) and gaussian dispersion (σ) about that angle

$$n[\alpha] = e^{-(1/2) ((\alpha - \theta_0)/\sigma)^2} \sin[\alpha],$$

or 2) two populations of probes, one perfectly ordered with an axial angle (θ), as would occur in an ideal helical structure, and the other completely disordered (i.e., isotropic). The proportion of disordered probes is termed f . In both models all of the probes have subnanosecond mobility in a cone of half-angle δ (Ling et al., 1996). Neither model is a realistic description of the probe orientation distribution, which would require more detailed information than currently available, but they are simple representations, indicating the angle of the major oriented component of the distribution while incorporating the types of disorder that may be present in a muscle fiber. Both of the simplified orientation distributions are described by three parameters (θ_0 , σ , and δ for model 1 or θ , f , and δ for model 2), whereas only two polarization ratios (Q_{\parallel} and Q_{\perp}) were determined at high time resolution in the experiments. However, δ (the half-angle of the cone in which the probes wobble on the subnanosecond time scale) is approximately 20° , as determined by independent measurements discussed above, and probably does not vary between physiological states. We fitted the two models to the steady-state Q ratios with δ set to 20° ; the effects of different values of δ on the fitted parameters are considered below (Figs. 9 and 10).

The Q ratios in rigor are consistent with a single population of probes with gaussian peak angle $\theta_0 = 63^\circ$ and dispersion $\sigma = \pm 23^\circ$ (Table 2). Interpreted in terms of two populations (helix plus isotropic model), the rigor Q ratios indicate about 55% of the probes could have an axial angle of 68° if the remaining 45% were isotropic (Table 2). Fluorescence polarization of fibers decorated with exogenous myosin subfragment 1 incorporating ATR-labeled cgRLC indicates similar disorder (Ling et al., 1996). Orientational disorder of the light-chain region is expected because in three-dimensional electron micrographic reconstructions of decorated thin filaments, the density of the RLC region is low (Milligan and Flicker, 1987), probably indicating disorder caused by flexibility within the myosin head. For the endogenous myosin heads the incommensu-

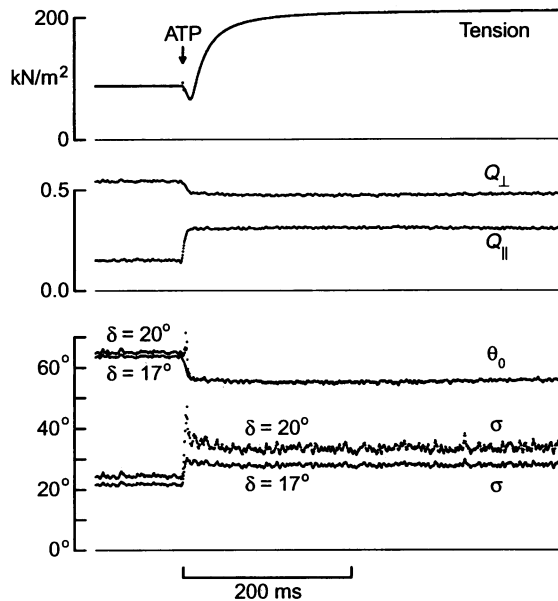


FIGURE 9 Time course of changes in probe orientation distributions determined by fitting fluorescence polarization transients with the gaussian model as described in text. The tension and Q signals were averaged to improve the signal-to-noise ratio, using eight photolysis trials (four fibers) with approximately 2 mM released [ATP]. The probe orientation distribution was modeled as a single population with an average angle (θ_0) and gaussian dispersion (σ) about that angle

$$n[\alpha] = e^{-(1/2)((\alpha-\theta_0)/\sigma)^2} \sin[\alpha].$$

This distribution was successively fitted to the Q_{\parallel} and Q_{\perp} values at each time point using a script written in MathCad. The model allows for free mobility of the probes in a cone of semi-angle δ on the time scale of the fluorescence lifetime. Because δ is not known accurately, the fitting procedure was conducted for $\delta = 17^\circ$ and 20° . The resulting time courses of σ and θ_0 are plotted in the lower panel. The transient behavior depends on the choice of δ , but for both values of δ , σ increases and θ_0 decreases on release of ATP.

rate periodicities between the two sets of filaments (Huxley and Brown, 1967) lead to varying strain among the cross-bridges, and in double-headed attachments the leading and trailing myosin heads are probably at different angles (Taylor et al., 1989). This point is discussed further in Ling et al. (1996). Adding Ca^{2+} or caged ATP to the rigor solution had little effect on the polarization ratios and, consequently, on the fitted model distributions (Table 2).

Disorder of the orientation distribution was higher in relaxing solution; both σ and f were larger than in rigor (Table 2). Disorder among cross-bridge angles in relaxed muscle has been commonly inferred from studies using extrinsic probes either at Cys 707 (Thomas and Cooke, 1980; Tanner et al., 1992) or at the RLC (Hambly et al., 1991, 1992; Ling et al., 1996), despite the ordered cross-bridge array observed in relaxed rabbit muscle at this temperature by x-ray diffraction (Lowy et al., 1991) and by electron microscopy (Ip and Heuser, 1983; Kensler et al., 1994; Sosa et al., 1994). Exchange of the labeled exogenous RLC for the endogenous protein apparently contributed to

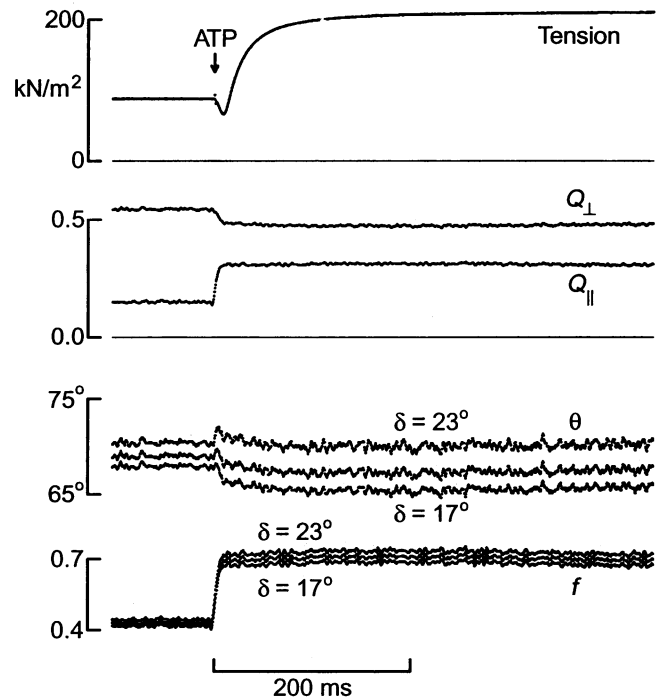


FIGURE 10 Time course of changes in probe orientation distributions determined by fitting fluorescence polarization transients with the helix plus isotropic model. The tension and Q signals are the same as in Fig. 9. The orientation distributions (model 2 described in the text) assume two populations of probes, one perfectly ordered with axial angle (θ) and the other completely disordered, i.e., isotropic. The proportion of disordered probes is denoted by f . This model also allows for free mobility of the probes in a cone of semi-angle δ on the time scale of the fluorescence lifetime, and the fitting procedure was carried out for $\delta = 17^\circ$, 20° , and 23° . The resulting time courses of f and θ are plotted in the lower panel. For all three values of δ , f increases on release of ATP. The time course of θ depends on the choice of δ , but the amplitudes are small (note expanded scale of θ compared with that for θ_0 in Fig. 9).

the disorder of the relaxed fibers in the present experiments (Ling et al., 1996). We found small but reproducible changes in the polarization ratios and model distributions when we added caged ATP or altered the ATP concentration in relaxing solution (Table 2). Surprisingly, reducing [ATP] increased disorder, which was the opposite of the change from relaxation to rigor. Adding caged ATP caused a slight decrease in disorder. Fitting the model orientation distributions to the polarization data after photolysis of caged ATP in the absence of Ca^{2+} shows that the probes were as disordered as in relaxing solution (e.g., compare 2' post-photolysis in Table 3 with Relax, 0.75 mM ATP + caged ATP in Table 2).

In active contraction initiated by caged ATP photolysis (Table 3) the gaussian model gave $55 \pm 33^\circ$, and the helix plus isotropic model indicated 29% of the probes with an axial angle of 67° and the remaining 71% isotropic. Both models suggest a substantial decrease in the orientational order when the fibers undergo the transition between rigor and active contraction, but not much change in preferred orientation, especially in the helix plus isotropic model.

This behavior is consistent with electron paramagnetic resonance studies in fibers using spin labels bound to rabbit skeletal RLC (mainly on Cys 125; Hambly et al., 1991, 1992) and bound to Cys 707 of the myosin heavy chain (Cooke et al., 1982). Electron microscopic studies also show that cross-bridges are less ordered during active contraction than in rigor (Tsukita and Yano, 1985; Hirose et al., 1993).

Fitting of model distributions to the polarization ratio signals

These two simple models for the probe orientation distribution were used to help interpret the transient changes in Q signals after photolysis of caged ATP in the presence of Ca^{2+} . Recordings from eight photolysis trials with approximately 2 mM [ATP] released were averaged to improve signal-to-noise ratio, and the model distributions were successively fitted to the Q_{\parallel} and Q_{\perp} values at each time point. As mentioned earlier, the most likely value for the half-width (δ) of the cone in which the probes undergo rapid motion is 20° , but the fitting procedure was repeated for a range of δ values to test the effect of varying this parameter.

In the gaussian model (Fig. 9), the peak angle (θ_0) decreased after the release of ATP and the dispersion (σ) increased, both by about 10° . With $\delta = 17^\circ$ (or lower, not shown), both deflections were monotonic; the increase of σ was slightly faster (half-time 3 ms) than the decrease of θ_0 (half-time 5.5 ms). With $\delta = 20^\circ$, both θ_0 and σ initially overshoot their final active contraction values. The gaussian model could not be fitted to the data with $\delta = 23^\circ$ or higher.

The helix plus isotropic model (Fig. 10) showed a rapid (half-time 4 ms) increase of f , the fraction of isotropic probes, for δ in the range 17 – 23° . Changes of the angle (θ) of the helically ordered component after photolysis were very small (less than $\sim 3^\circ$), but the time course depended on δ . The initial fast component of the change in θ was an increase at $\delta = 20^\circ$ and 23° but a decrease (half-time 7.5 ms) at $\delta = 17^\circ$. At all three values of δ shown, θ then decreased slightly with a time course similar to that of the rise of tension (Fig. 10), before slowly increasing again during the next second. (Only the initial part of the latter component is visible in Fig. 10.) At $\delta < 17^\circ$, the time courses of θ and f were very similar to those at $\delta = 17^\circ$. Qualitatively similar but slower time courses for the fitted parameters in both models were obtained by fitting to Q signals obtained at lower (200 μM) [ATP].

Fitting these simple models to the time course of the Q signals shows that, within 3–4 ms after the laser pulse, binding of ATP to the myosin heads causes disordering of the probe orientation distribution. The time course for the peak angle of the ordered component is uncertain because this depends on the specific model distribution chosen as well as the assumed extent (δ) of subnanosecond probe motion. For both models, with δ at values low enough ($\leq 20^\circ$) to avoid fast biphasic deflections, the peak angle (θ_0

or θ) changed slightly more slowly than the increase of disorder (σ or f), accounting for the slightly slower time course we observed for Q_{\perp} after photolysis compared to Q_{\parallel} (Figs. 2–6). In general, the observation of more than one time course in the optical signals indicates several kinetic processes in the binding of ATP, dissociation of myosin from actin, reattachment, and subsequent force generation. The earliest event detectable with the present signals, independent of the model chosen and the extent of subnanosecond motion, is a disordering of the probes, and presumably the underlying light-chain region, with a half-time 3–4 ms after the laser pulse.

Kinetics of fluorescence polarization signals after ATP release: comparison with other time-resolved structural measurements

The fast changes in the Q signals and in the orientation distribution of the RLC probes after ATP release, with reciprocal half-times of 100 – 300 s^{-1} at 2 mM ATP, correspond to apparent second-order rate constants between 10^5 and $10^6 \text{ M}^{-1} \text{ s}^{-1}$ (Fig. 4 B). Fast movements of myosin heads after ATP release in rigor fibers from rabbit psoas muscle have been demonstrated previously by several other techniques. Linear dichroism and fluorescence polarization from ATR probes on Cys 707 of the myosin heavy chain change with an apparent second-order rate constant of 1 – $5 \times 10^5 \text{ M}^{-1} \text{ s}^{-1}$ (20°C ; Tanner et al., 1992; C. L. Berger and Y. E. Goldman, personal communication), similar to that found here for the change in the orientation of the light-chain region of the head. The main deflections of the fluorescence signals from probes at both sites are temporally dissociated from force generation. However, the average orientation of ATR probes on Cys 707 changes rapidly by a similar amount on release of either ATP or ADP (Tanner et al., 1992; Berger et al., 1995). In contrast, ATR on cgRLC gives only small signals on ADP release (Fig. 8), in the direction opposite those produced by ATP release (Figs. 2 and 5), indicating that the deflections obtained on photolysis of caged ATP are specific effects of ATP. The present results show that the local structural change associated with nucleotide binding, sensed by ATR on Cys 707, is accompanied by large movements of the light-chain region for binding of ATP but not ADP. In the ATR-Cys-707 experiments, as in the present results, there is some evidence for smaller changes of probe orientation during the onset of active force development.

The intensities of the inner equatorial x-ray reflections, which are sensitive to the radial distribution of mass between the thick and thin filaments, also show large, fast changes after ATP release in rigor fibers (Poole et al., 1988, 1991; Brown et al., 1995). In the absence of Ca^{2+} , the change in the equatorial intensities has a reciprocal half-time greater than 1000 s^{-1} , corresponding to an apparent second-order rate constant greater than $10^6 \text{ M}^{-1} \text{ s}^{-1}$ (2 mM ATP released at 24°C ; Poole et al., 1988, 1991). At 5°C the

reciprocal half-time is 170 s^{-1} (1 mM ATP released from dimethoxybenzoin (DMB) caged ATP; Brown et al., 1995). When ATP is released in the presence of Ca^{2+} the reciprocal half-times are greater than 200 s^{-1} at 24°C ($>2 \text{ mM}$ ATP released; Poole et al., 1991), and 160 s^{-1} at 5°C (1 mM ATP released from DMB caged ATP; Brown et al., 1995). These rapid changes have generally been interpreted on the basis of detachment of myosin heads from actin, but changes in the conformation of attached heads could also contribute to the mass transfer. Small components of equatorial intensity changes accompany the slower final relaxation in the absence of Ca^{2+} , but there is no clear component concomitant with force development in the presence of Ca^{2+} .

Muscle fiber birefringence changes rapidly after release of ATP in the absence of Ca^{2+} , indicating a change in the mean orientation of the myosin heads (Peckham et al., 1994). The fast component of the birefringence change has a reciprocal half-time of 90 s^{-1} at 100 mM ionic strength, 15°C . A slower component of the birefringence signal accompanies final relaxation. The slow component constitutes a larger fraction of the overall change for the birefringence signal than for the signals obtained with the other methods.

All of these millisecond time-resolved structural methods show movements of the myosin heads after ATP release with reciprocal half-times of about 100 s^{-1} or greater, depending on experimental conditions. Taken together the results show that a large-scale motion of the head, including a change in orientation of the light-chain region, occurs promptly on binding of ATP.

Transitions in the cross-bridge cycle corresponding to the orientation changes

The second-order rate constants for changes of fluorescence polarization ($1\text{--}5 \times 10^5 \text{ M}^{-1} \text{ s}^{-1}$ for Q_{\perp} and $3\text{--}10 \times 10^5 \text{ M}^{-1} \text{ s}^{-1}$ for Q_{\parallel} ; Figs. 4 B and 6) are somewhat lower than the second-order rate constant for detachment of myosin subfragment 1 by ATP from actin in solution ($\sim 20 \times 10^5 \text{ M}^{-1} \text{ s}^{-1}$; White and Taylor, 1976). Some of this difference can be attributed to binding of ADP or caged ATP to the cross-bridges, which would slow binding of photoreleased ATP (Thirlwell et al., 1994, 1995). Thus the changes in the orientation distribution indicated by the Q signals are associated with very early events after ATP binding.

One such early event is cross-bridge detachment, as shown by the rapid decline of tension and stiffness (Figs. 2, 3, and 5). We sought to determine the temporal relationship between the fluorescence polarization changes and cross-bridge detachment by using an experimental protocol developed in earlier studies (Goldman et al., 1984a,b) to monitor detachment. Assuming that an increment of cross-bridge strain introduced by a length step in rigor would disappear immediately on detachment of the cross-bridge, the convergence of paired tension traces starting from different rigor tensions (Figs. 1, 5, and 7) has been interpreted

as the time course of detachment of the original rigor cross-bridges (Goldman et al., 1984a,b). The tension traces converged more slowly than the major change of the fluorescence polarization ratios (Figs. 5 and 7), and the second-order rate constant of $0.5\text{--}2 \times 10^5 \text{ M}^{-1} \text{ s}^{-1}$ for tension convergence was lower than those for the Q traces (Fig. 6). If the additional strain imposed on the cross-bridges by a stretch in rigor is indeed lost immediately on detaching from actin, then the faster deflections of the Q signals imply that changes in orientation of the light-chain region of the myosin heads precede detachment. A difficulty with this interpretation is that the delay between the Q signals and tension convergence ($\sim 15 \text{ ms}$ at 1 mM ATP) is much longer than the lifetime ($<1 \text{ ms}$) of the actomyosin-ATP complex before dissociation from actin in solution (White and Taylor, 1976).

An alternative possibility is that deflections of the Q signals might accompany cross-bridge detachment rather than tension convergence. The tension traces might converge more slowly if an increment in applied strain was preserved during detachment and reattachment to a greater extent than the orientational order. For example, detachment of a single head of a myosin molecule might decrease tension less than it increases angular disorder. In support of some residual interaction between myosin heads and actin during the transient tension dip, the out-of-phase stiffness, which is a signal of quick stress relaxation or rapid attachment/detachment kinetics, rises markedly earlier than force (Horiuti et al., 1992; Figs. 2 and 3).

Thus the prompt deflections of the Q_{\parallel} and Q_{\perp} signals may accompany either ATP binding or the subsequent cross-bridge dissociation, but either case would require novel features of cross-bridge behavior.

Nearly steady polarization ratios during active force development

During the active force development phase after ATP release in the presence of Ca^{2+} , cross-bridges are thought to attach to actin and undergo a structural transition to the force-generating states. The fluorescence polarization ratios changed remarkably little during this period (Figs. 2 A, 5, 7). At low concentrations of photoliberated ATP, any changes in the Q ratios might be obscured by signal recovery associated with ATP depletion or accumulation of ADP (Fig. 3). However, when more than 1.7 mM ATP was released, the recovery of the Q traces was negligible during force development. Changes in Q ratios accompanying the force development phase were estimated to be $<15\%$ of the total signal change, indicating that angular changes of the light-chain region during force development are much less than those accompanying the earlier events of ATP binding and cross-bridge detachment. Most other structural methods that are sensitive to movements of the myosin heads have also shown little change during active force development after photolysis of caged ATP, including ATR probes on

Cys 707 of the myosin heavy chain (Tanner et al., 1992; Berger et al., 1995), equatorial x-ray diffraction (Poole et al., 1991; Brown et al., 1995), and electron microscopy (Hirose et al., 1993). However, the intensity of the 14.5-nm meridional x-ray reflection does seem to increase with a time course similar to that of active force development after photorelease of ATP (Poole et al., 1991).

The upper limit for the magnitude of Q signal changes during force development corresponds to an increase in Q_{\parallel} of about 0.02 and a decrease in Q_{\perp} of about 0.006. Interpreted in terms of the two models for the orientation distribution of probe dipoles considered above, these changes correspond to a decrease in the peak angle of the Gaussian distribution (θ_0) or the axial angle of the ordered fraction (θ) by about 2° or less (Figs. 9 and 10). Compared with the changes accompanying force development after a quick release (a decrease in Q_{\parallel} of about 0.007 and an increase in Q_{\perp} of about 0.022; Irving et al., 1995), the present deflections during force development are opposite in sign but roughly similar in magnitude or smaller. In both protocols force development by a large fraction of the isometric value seems to be accompanied by little change in the mean orientation of the myosin light-chain region.

There are many differences between the two protocols, and the rates of force generation differ by an order of magnitude, suggesting that they are limited by different kinetic steps. In the caged ATP protocol there may be substantial sarcomere shortening during force development, and the component of the signal change associated with force development per se was not reliably isolated from the much larger signal associated with ATP binding and/or cross-bridge detachment. Nevertheless, both sets of results seem inconsistent with a large change in the orientation of the light-chain region of the myosin heads during force development.

This observation is difficult to reconcile with conventional cross-bridge models in which tilting of the myosin heads produces a working stroke of about 10 nm (Huxley and Simmons, 1971). It seems unlikely that replacing endogenous RLCs by ATR-labeled chicken gizzard RLC suppresses crucial cross-bridge motions, because RLC-exchanged fibers give normal mechanical transients in both the caged ATP and length step protocols (Fig. 1 and Irving et al., 1995). It is also unlikely that the ATR-cgRLC probe is positioned at an unfavorable orientation to detect the critical angle change, because preliminary results show similarly small angle changes when quick length changes were applied to fibers incorporating RLCs labeled at other sites engineered into the sequence (unpublished data of S. Hopkins, C. Sabido-David, L. Saraswat, S. Lowey, M. Irving, and Y. E. Goldman).

One explanation for the small signal changes during force generation might be that full isometric force is generated by a small fraction of the myosin heads in the fiber, whereas the polarization ratios represent an average over all of the heads. A problem with this hypothesis is that muscle stiff-

ness is relatively high during contraction (Goldman and Simmons, 1977; Higuchi et al., 1995).

Another possibility is that the rate of active force development is partly limited by filament sliding due to mechanical compliance either at the ends of the fibers or within the sarcomeres (H. E. Huxley et al., 1994; Wakabayashi et al., 1994; Higuchi et al., 1995). Actively force-generating cross-bridges may be present very soon after ATP release and may execute repeated force-generating impulses as the filaments slide during final tension development. If the orientation distribution during filament sliding were similar to that in isometric contraction, the Q signals would be steady during this period. The force-generating transitions would be repeated several times faster than the rate of ATP splitting (2 s^{-1} at 12°C ; Ferenczi et al., 1984), implying loose coupling between the biochemical and mechanical cycles, as suggested from other experiments (Yanagida et al., 1985; Higuchi and Goldman, 1991; 1995; Lombardi et al., 1992).

A third possible explanation is that the probe orientation distribution is so broad that it spans the plane perpendicular to the fiber axis (equatorial plane). The critical structural change associated with force generation would then tilt some of the probes toward the equatorial plane and the rest away from it. In this case the net change observed by the fluorescence polarization method, which does not distinguish between axial angles on the two sides of this plane (a and $180^\circ - a$), would appear to be small. In support of this idea, the observed polarization ratios during isometric contraction are consistent with a high degree of orientational disorder (Table 2; Figs. 9 and 10; Ling et al., 1996). Furthermore, Irving et al. (1995) found that response of the polarization signals to length steps had opposite signs in rigor and in active contraction, suggesting that the major probe orientations in these two states are on opposite sides of the equatorial plane. This idea predicts that the main probe orientation should traverse the equatorial plane in the transition from rigor to active contraction initiated by photorelease of ATP in the present experiments. There is a hint of such behavior in some of the model fits showing a transient overshoot of θ_0 and θ (Figs. 9 and 10), but several factors would limit the detectability of a possible transient 90° state in the present experiments, including the initial disorder of probe angles, the incomplete synchronization of ATP binding and detachment among cross-bridges, and the unknown orientation distribution of the heads briefly detached during the transient. The response to length changes during transients initiated by caged ATP photolysis might help characterize the hypothetical low-force cross-bridges just after reattachment (Hopkins et al., 1995).

In summary, we observed angle changes in a fluorescent probe placed on the regulatory light chains of myosin in rabbit psoas fibers when a rigor muscle was suddenly activated by photorelease of ATP from caged ATP. An apparent disordering occurred promptly, accompanying either ATP binding or cross-bridge detachment, but before active force development. Such disordering was not observed on pho-

tolysis of caged ADP. Several factors may reduce the changes in fluorescence polarization during force development, including the multiplicity of cross-bridge states, filament sliding, and orientational disorder, which may span the equatorial plane.

We thank Joe Pili for skilled mechanical design and construction and Marcus Bell for software support.

The work was supported by NIH grant AR26846 to YEG, Wellcome Trust UK grant 033813 to MI, the UK Medical Research Council, and the Muscular Dystrophy Associations of America.

REFERENCES

- Allen, T. St. C., N. Ling, Y. E. Goldman, and M. Irving. 1992. Structural changes of myosin light chain 2 in skinned muscle fibers following photolysis of caged ATP and ADP. *Biophys. J.* 61:286a. (Abstr.)
- Allen, T. St. C., N. Ling, Y. E. Goldman, and M. Irving. 1993. Kinetics of orientation changes of rhodamine probes on myosin regulatory light chains in skinned muscle fibers following photolysis of caged ATP. *Biophys. J.* 64:231a. (Abstr.)
- Barabas, K., and L. Keszthelyi. 1984. Temperature dependence of ATP release from "caged" ATP. *Acta Biochim. Biophys. Acad. Sci. Hung.* 19:305–309.
- Berger, C. L., J. S. Craik, D. R. Trentham, J. E. T. Corrie, and Y. E. Goldman. 1995. Fluorescence polarization from isomers of tetramethylrhodamine at SH-1 in rabbit psoas muscle fibers. *Biophys. J.* 68:78s–80s.
- Brown, P. D., M. A. Ferenczi, M. Irving, and I. Dobbie. 1995. Time course of tension and intensities of the inner equatorial x-ray reflections on the photolysis of DMB-caged ATP in apyrase-treated rabbit skeletal muscle fibres. *Biophys. J.* 68:67a. (Abstr.)
- Burghardt, T. P., T. Ando, and J. Borejdo. 1983. Evidence for cross-bridge order in contraction of glycerinated skeletal muscle. *Proc. Natl. Acad. Sci. USA.* 80:7515–7519.
- Chase, P. B., D. A. Martyn, M. J. Kushmerick, and A. M. Gordon. 1993. Effects of inorganic phosphate analogues on stiffness and unloaded shortening of skinned muscle fibres from rabbit. *J. Physiol.* 460:231–246.
- Chen, R. F., and R. L. Bowman. 1965. Fluorescence polarization: measurement with ultraviolet-polarizing filters in a spectrophotofluorometer. *Science.* 147:729–732.
- Cooke, R. 1986. The mechanism of muscle contraction. *CRC Crit. Rev. Biochem.* 21:53–118.
- Cooke, R., M. S. Crowder, and D. D. Thomas. 1982. Orientation of spin labels attached to cross-bridges in contracting muscle fibres. *Nature.* 300:776–778.
- Corrie, J. E. T., and J. S. Craik. 1994. Synthesis and characterisation of pure isomers of iodoacetamidotetramethylrhodamine. *J. Chem. Soc. Perkin Trans.* 1:2967–2973.
- Dantzig, J. A., M. G. Hibberd, D. R. Trentham, and Y. E. Goldman. 1991. Cross-bridge kinetics in the presence of MgADP investigated by photolysis of caged ATP in rabbit psoas muscle fibres. *J. Physiol.* 432:639–680.
- Ferenczi, M. A. 1986. Phosphate burst in permeable muscle fibers of the rabbit. *Biophys. J.* 50:471–477.
- Ferenczi, M. A., E. Homsher, and D. R. Trentham. 1984. The kinetics of magnesium-adenosine triphosphate cleavage in skinned muscle fibers of the rabbit. *J. Physiol.* 352:575–599.
- Fisher, A. J., C. A. Smith, J. Thoden, R. Smith, K. Sutoh, H. M. Holden, and I. Rayment. 1995. Structural studies of myosin: nucleotide complexes: a revised model for the molecular basis of muscle contraction. *Biophys. J.* 68:19s–28s.
- Goldman, Y. E., M. G. Hibberd, J. A. McCray, and D. R. Trentham. 1982. Relaxation of muscle fibres by photolysis of caged ATP. *Nature.* 300:701–705.
- Goldman, Y. E., M. G. Hibberd, and D. R. Trentham. 1984a. Relaxation of rabbit psoas muscle fibres from rigor by photochemical generation of adenosine-5'-triphosphate. *J. Physiol.* 354:577–604.
- Goldman, Y. E., M. G. Hibberd, and D. R. Trentham. 1984b. Initiation of active contraction by photogeneration of adenosine-5'-triphosphate in rabbit psoas muscle fibres. *J. Physiol.* 354:605–624.
- Goldman, Y. E., and R. M. Simmons. 1977. Active and rigor muscle stiffness. *J. Physiol.* 269:55–57P.
- Goldman, Y. E., and R. M. Simmons. 1984. Control of sarcomere length in skinned muscle fibres of *Rana temporaria* during mechanical transients. *J. Physiol.* 350:497–518.
- Gutfreund, H. 1972. Transients and relaxation. In *Enzymes: Physical Principles*. John Wiley and Sons, London. 176–228.
- Hambly, B., K. Franks, and R. Cooke. 1991. Orientation of spin-labeled light chain-2 exchanged onto myosin cross-bridges in glycerinated muscle fibers. *Biophys. J.* 59:127–138.
- Hambly, B., K. Franks, and R. Cooke. 1992. Paramagnetic probes attached to a light chain on the myosin head are highly disordered in active muscle fibers. *Biophys. J.* 63:1306–1313.
- Higuchi, H., and Y. E. Goldman. 1991. Sliding distance between actin and myosin filaments per ATP molecule hydrolysed in skinned muscle fibres. *Nature.* 352:352–354.
- Higuchi, H., and Y. E. Goldman. 1995. Sliding distance per ATP molecule hydrolyzed by myosin heads during isotonic shortening of skinned muscle fibers. *Biophys. J.* 69:1491–1507.
- Higuchi, H., T. Yanagida, and Y. E. Goldman. 1995. Compliance of thin filaments in skinned fibers of rabbit skeletal muscle. *Biophys. J.* 69:1000–1010.
- Hirose, K., C. Franzini-Armstrong, Y. E. Goldman, and J. M. Murray. 1994. Structural changes in muscle crossbridges accompanying force generation. *J. Cell Biol.* 127:763–778.
- Hirose, K., T. D. Lenart, J. M. Murray, C. Franzini-Armstrong, and Y. E. Goldman. 1993. Flash and smash: rapid freezing of muscle fibers activated by photolysis of caged ATP. *Biophys. J.* 65:397–408.
- Homsher, E., and N. C. Millar. 1990. Caged compounds and striated muscle contraction. *Annu. Rev. Physiol.* 52:875–896.
- Hopkins, S. C., L. Phan, M. Irving, and Y. E. Goldman. 1995. Oscillations in the orientation of acetamidotetramethylrhodamine (ATR) probes on myosin regulatory light chain (RLC) caused by sinusoidal length changes in skinned muscle fibers. *Biophys. J.* 66:9a. (Abstr.)
- Horiuti, K., T. Sakoda, and K. Yamada. 1992. Time course of rise of muscle stiffness at onset of contraction induced by photorelease of ATP. *J. Muscle Res. Cell Motil.* 13:685–691.
- Huxley, A. F., and R. M. Simmons. 1971. Proposed mechanism of force generation in striated muscle. *Nature.* 233:533–538.
- Huxley, H. E. 1969. The mechanism of muscular contraction. *Science.* 164:1356–1366.
- Huxley, H. E., and W. Brown. 1967. The low-angle x-ray diagram of vertebrate skeletal muscle and its behaviour during contraction and rigor. *J. Mol. Biol.* 30:383–434.
- Huxley, H. E., A. Stewart, H. Sosa, and T. Irving. 1994. X-ray diffraction measurements of the extensibility of actin and myosin filaments in contracting muscle. *Biophys. J.* 67:2411–2421.
- Ip, W., and J. Heuser. 1983. Direct visualization of the myosin crossbridge helices on relaxed rabbit psoas thick filaments. *J. Mol. Biol.* 171:105–109.
- Irving, M. 1996. Steady-state polarization from cylindrically-symmetric fluorophores undergoing rapid restricted motion. *Biophys. J.* 70:1830–1835.
- Irving, M., T. St. C. Allen, C. Sabido-David, J. S. Craik, B. Brandmeier, J. Kendrick-Jones, J. E. T. Corrie, D. R. Trentham, and Y. E. Goldman. 1995. Tilting of the light-chain region of myosin during step length changes and active force generation in skeletal muscle. *Nature.* 375:688–691.
- Kensler, R. W., S. Peterson, and M. Norberg. 1994. The effects of changes in temperature or ionic strength on isolated rabbit and fish skeletal muscle thick filaments. *J. Muscle Res. Cell Motil.* 15:69–79.
- Ling, N., C. Shrimpton, J. Sleep, J. Kendrick-Jones, and M. Irving. 1996. Fluorescent probes of the orientation of myosin regulatory light chains in relaxed, rigor and contracting muscle. *Biophys. J.* 70:1836–1846.

- Lombardi, V. G. Piazzesi, and M. Linari. 1992. Rapid regeneration of the actin-myosin power stroke in contracting muscle. *Nature*. 355:638–641.
- Lowy, J., D. Popp, and A. A. Stewart. 1991. X-ray studies of order-disorder transitions in the myosin heads of skinned rabbit psoas muscles. *Biophys. J.* 60:812–824.
- Lymn, R. W., and E. W. Taylor. 1971. Mechanism of adenosine triphosphate hydrolysis by actomyosin. *Biochemistry*. 10:4617–4624.
- Milligan, R. A., and P. F. Flicker. 1987. Structural relationships of actin, myosin, and tropomyosin revealed by cryo-electron microscopy. *J. Cell Biol.* 105:29–39.
- Moss, R. L., G. G. Giulian, and M. L. Greaser. 1982. Physiological effects accompanying the removal of myosin LC2 from skinned skeletal muscle fibers. *J. Biol. Chem.* 257:8588–8591.
- Ostap, E. M., V. A. Barnett, and D. D. Thomas. 1995. Resolution of three structural states of spin-labeled myosin in contracting muscle. *Biophys. J.* 69:177–188.
- Peckham, M., M. A. Ferenczi, and M. Irving. 1994. A birefringence study of changes in myosin orientation during relaxation of skinned muscle fibers induced by photolytic ATP release. *Biophys. J.* 67:1141–1148.
- Poole, K. J. V., Y. Maeda, G. Rapp, and R. S. Goody. 1991. Dynamic x-ray diffraction measurements following photolytic relaxation and activation of skinned rabbit psoas fibres. *Adv. Biophys.* 27:63–75.
- Poole, K. J. V., G. Rapp, Y. Maéda, and R. S. Goody. 1988. The time course of changes in the equatorial diffraction patterns from different muscle types on photolysis of caged-ATP. In *Advances In Experimental Medicine and Biological Molecular Mechanism of Muscle Contraction*, Vol. 226. H. Sugi and G. Pollack, editors. Plenum Press, New York. 391–404.
- Press, W. H., S. A. Teukolsky, W. T. Vetterling, and B. P. Flannery. 1992. Nonlinear models. In *Numerical Recipes in C: The Art of Scientific Computing*, 2nd ed. Cambridge University Press, New York. 683–688.
- Rader, C. M., and B. Gold. 1967. Digital filter design techniques in the frequency domain. *Proc. IEEE*. 55:149–171.
- Rayment, I., H. M. Holden, M. Whittaker, C. B. Yohn, M. Lorenz, K. C. Holmes, and R. A. Milligan. 1993. Structure of the actin-myosin complex and its implications for muscle contraction. *Science*. 261:58–65.
- Reedy, M. K., R. S. Goody, W. Hofmann, and G. Rosenbaum. 1983. Co-ordinated electron microscopy and x-ray studies of glycerinated insect flight muscle. I. X-ray diffraction monitoring during preparation for electron microscopy of muscle fibres fixed in rigor, in ATP and in AMPPNP. *J. Muscle Res. Cell Motil.* 4:25–53.
- Reedy, M. K., K. C. Holmes, and R. T. Tregear. 1965. Induced changes in orientation of the cross-bridges of glycerinated insect flight muscle. *Nature*. 207:1276–1280.
- Sabido-David, C., J. S. Craik, B. Brandmeier, J. E. T. Corrie, D. R. Trentham, N. Ling, and M. Irving. 1994. Orientation of acetamidotetramethylrhodamine (ATR) isomers covalently bound to regulatory light chains in rabbit psoas muscle fibers. *Biophys. J.* 66:234a. (Abstr.)
- Savitzky, A., and M. J. E. Golay. 1964. Smoothing and differentiation of data by simplified least squares procedures. *Anal. Chem.* 36:1627–1639.
- Sosa, H., D. Popp, G. Ouyang, and H. E. Huxley. 1994. Ultrastructure of skeletal muscle fibers studied by a plunge quick freezing method: myofilament lengths. *Biophys. J.* 67:283–292.
- Tanner, J. W., D. D. Thomas, and Y. E. Goldman. 1992. Transients in orientation of a fluorescent cross-bridge probe following photolysis of caged nucleotides in skeletal muscle fibres. *J. Mol. Biol.* 223:185–203.
- Taylor, K. A., M. C. Reedy, L. Cordova, and M. K. Reedy. 1989. Three-dimensional image reconstruction of insect flight muscle. II. The rigor actin layer. *J. Cell Biol.* 109:1103–1123.
- Thirlwell, H., J. E. T. Corrie, G. P. Reid, D. R. Trentham, and M. A. Ferenczi. 1994. Kinetics of relaxation from rigor of permeabilized fast-twitch skeletal fibers from the rabbit using a novel caged ATP and apyrase. *Biophys. J.* 67:2436–2447.
- Thirlwell, H., J. A. Sleep, and M. A. Ferenczi. 1995. Inhibition of unloaded shortening velocity in permeabilized muscle fibres by caged ATP compounds. *J. Muscle Res. Cell Motil.* 16:131–137.
- Thomas, D. D. 1987. Spectroscopic probes of muscle cross-bridge rotation. *Annu. Rev. Physiol.* 49:691–709.
- Thomas, D. D., and R. Cooke. 1980. Orientation of spin-labeled myosin heads in glycerinated muscle fibers. *Biophys. J.* 32:891–906.
- Tsukita, S., and M. Yano. 1985. Actomyosin structure in contracting muscle detected by rapid freezing. *Nature*. 317:182–184.
- Vibert, P., and C. Cohen. 1988. Domains, motions and regulation in the myosin head. *J. Muscle Res. Cell Motil.* 9:296–305.
- Wakabayashi, K., Y. Sugimoto, H. Tanaka, Y. Ueno, Y. Takezawa, and Y. Amemiya. 1994. X-ray diffraction evidence for the extensibility of actin and myosin filaments during muscle contraction. *Biophys. J.* 67:2422–2435.
- Walker, J. W., G. P. Reid, J. A. McCray, and D. R. Trentham. 1988. Photolabile 1-(2-Nitrophenyl)ethyl phosphate esters of adenine nucleotide analogues. Synthesis and mechanism of photolysis. *J. Am. Chem. Soc.* 110:7170–7177.
- Weber, G. 1952. Polarization of the fluorescence of macromolecules 1. Theory and experimental method. *Biochemistry*. 51:145–155.
- White, H. D., and E. W. Taylor. 1976. Energetics and mechanism of actomyosin adenosine triphosphatase. *Biochemistry*. 15:5818–5826.
- Yanagida, T., T. Arata, and F. Oosawa. 1985. Sliding distance of actin filament induced by a myosin crossbridge during one ATP hydrolysis cycle. *Nature*. 316:366–369.
- Yount, R. G. 1975. ATP analogs. *Adv. Enzymol.* 43:1–56.